Detailed structure of the tropical upper troposphere and lower stratosphere as revealed by balloon sonde observations of water vapor, ozone, temperature, and winds during the NASA TCSP and TC4 campaigns

Henry B. Selkirk,[1] Holger Vömel,[2] Jéssica María Valverde Canossa,[3] Leonhard Pfister,[4] Jorge Andrés Diaz,[5] Walter Fernández,[5] Jorge Amador,[5,6] Werner Stolz,[7] and Grace S. Peng[8]

Received 18 September 2009; revised 14 April 2010; accepted 20 April 2010; published 21 September 2010.

[1] We report on balloon sonde measurements of water vapor and ozone using the cryogenic frost point hygrometer and electrochemical concentration cell ozonesondes made at Alajuela, Costa Rica (10.0°N, 84.2°W) during two NASA airborne campaigns: the Tropical Convective Systems and Processes (TCSP) mission in July 2005 and the Tropical Composition, Clouds, and Climate Coupling Experiment (TC4), July–August 2007. In both campaigns we found an upper troposphere that was frequently supersaturated but no evidence that deep convection had reached the tropopause. The balloon sondes were complemented by campaigns of 4 times daily high-resolution radiosondes from mid-June through mid-August in both years. The radiosonde data reveal vertically propagating equatorial waves that caused a large increase in the variability of temperature in the tropical tropopause layer (TTL). These waves episodically produced cold point tropopauses (CPTs) above 18 km, yet in neither campaign was saturation observed above ~380 K or 17 km. The averages of the water vapor minima below this level were 5.2 ppmv in TCSP and 4.8 ppmv in TC4, and the individual profile minima all lay at or above ~360 K. The average minima in this 360–380 K layer provide a better estimate of the effective stratospheric entry value than the average mixing ratio at the CPT. We refer to this upper portion of the TTL as the tropopause saturation layer and consider it to be the locus of the final dehydration of nascent stratospheric air. As such, it is the local equivalent to the tape head of the water vapor tape recorder.

Citation: Selkirk, H. B., H. Vömel, J. M. Valverde Canossa, L. Pfister, J. A. Diaz, W. Fernández, J. Amador, W. Stolz, and G. S. Peng (2010), Detailed structure of the tropical upper troposphere and lower stratosphere as revealed by balloon sonde observations of water vapor, ozone, temperature, and winds during the NASA TCSP and TC4 campaigns, *J. Geophys. Res.*, *115*, D00J19, doi:10.1029/2009JD013209.

1. Introduction

[2] The means by which water vapor is dehydrated and transported into the tropical lower stratosphere has been a very lively subject of debate since *Danielsen* [1982] and *Newell and Gould-Stewart* [1981] presented different views of the relative roles of deep convection and of large-scale lifting and radiative heating in tropical stratosphere-troposphere exchange. These papers were motivated in part by observations of the annual cycle of tropical tropopause temperature and its relationship to the spatial and seasonal distribution of deep convection in the tropics [*Reed and Vleck*, 1969; *Reid and Gage*, 1981; *Yulaeva et al.*, 1994; *Reid and Gage*, 1996]. *Mote et al.* [1996] first showed that the annual cycle of the temperature at the tropical tropopause imprints a coherent signal on the water vapor content in the tropical stratosphere. This observation and subsequent refinements using much longer satellite records impose powerful constraints on estimates of the tropical upwelling rate and the mixing into the tropics from the middle latitudes [*Mote et al.*, 1998; *Schoeberl et al.*, 2008]. They also bear on estimates of the effective mixing ratio of water as it passes irreversibly through the tropical tropopause and enters the tropical stratospheric "pipe" [*Plumb and Ko*, 1992].

[1]Goddard Earth Sciences and Technology Center, University of Maryland Baltimore County, Baltimore, Maryland, USA.
[2]Deutscher Wetterdienst, Meteorologisches Observatorium, Lindenburg, Germany.
[3]School of Environmental Sciences, National University, Heredia, Costa Rica.
[4]Earth Sciences Division, NASA Ames Research Center, Moffett Field, California, USA.
[5]School of Physics, University of Costa Rica, San Jose, Costa Rica.
[6]Center for Geophysical Research, University of Costa Rica, San Jose, Costa Rica.
[7]National Meteorological Institute, San Jose, Costa Rica.
[8]The Aerospace Corporation, Los Angeles, California, USA.

Copyright 2010 by the American Geophysical Union.
0148-0227/10/2009JD013209

[3] Despite these advances in our understanding of the large-scale circulation in the tropical stratosphere, the remoteness of the tropical tropopause environment makes direct observation of the physical processes that lead to dehydration and troposphere-to-stratosphere exchange (TSE) difficult. Nevertheless, as shown by *Wang et al.* [1996], thin cirrus are present at or near the tropopause over large regions of the tropics year round, and *Gettelman et al.* [2002] and *Liu and Zipser* [2005] demonstrated that deep convective ascent to and through the tropical tropopause is relatively rare. These observations provide support for a range of TSE processes occurring on scales greater than the convective in the tropical tropopause layer or TTL [*Highwood and Hoskins*, 1998; *Gettelman and Forster*, 2002; *Fueglistaler et al.*, 2009]. These larger-scale processes fundamentally rest on the net radiative heating in the upper part of the TTL [*Thuburn and Craig*, 2002]. *Sherwood and Dessler* [2001] stressed the need to satisfy the global balance of mass as well as those of water vapor, ozone, and other trace species. They advocated a TSE regime that is a mix of convective overshooting and slow ascent at larger scales, whereas *Corti et al.* [2006] proposed a more important role for radiative lofting of cloud layers in TTL.

[4] Dehydration and TSE by horizontal advection have been studied by *Jensen et al.* [1996], *Hartmann et al.* [2001], *Holton and Gettelman* [2001], and *Pfister et al.* [2001]. Results of investigations using Lagrangian approaches by *Jensen and Pfister* [2004], *Fueglistaler et al.* [2005], and *Fueglistaler and Haynes* [2005] support the idea that dehydration occurs in wave-driven episodes of adiabatic uplift in an overall environment of slow, diabatic ascent. Furthermore, increasing evidence from detailed modeling studies [e.g., *Jensen et al.*, 2007; *Grosvenor et al.*, 2007] and from observations [*Corti et al.*, 2008] suggests that deep convection is more likely to hydrate than dehydrate the TTL and lower stratosphere.

[5] *Vömel et al.* [2002] analyzed balloon sonde measurements of water vapor and ozone at diverse locations in the tropics, including the western Pacific warm pool, the eastern equatorial Pacific, and South America. They found supersaturation in the upper troposphere under a wide range of conditions and concluded that tropopause dehydration was occurring not only due to rapid ascent in deep convective systems but also through slow ascent and lifting by the passage of Kelvin waves [*Fujiwara et al.*, 2001].

[6] Some recent in situ observations from aircraft present a more complicated picture of the TTL. *MacKenzie et al.* [2006] report on the results of the Airborne Platform for Earth Observation (APE)- Third European Stratospheric Experiment on Ozone (THESEO) mission over the western equatorial Indian Ocean in February and March 1999 where deep convection had significant impact on the vertical structure near the tropopause on at least one flight. *Schiller et al.* [2009] present data from three recent airborne campaigns in widely varying convective environments: the 2005 Tropical Convection, Cirrus and Nitrogen Oxides Experiment (TROCCINOX) campaign in the interior of southern Brazil [*Konopka et al.*, 2007], the Stratospheric-Climate Links with Emphasis on the Upper Troposphere and Lower Stratosphere (SCOUT-O3)/Aerosol and Chemical Transport in Deep Convection (ACTIVE) campaign in late 2005 in northern Australia [*Vaughan et al.*, 2008], and the African Monsoon Multidisciplinary Analysis (AMMA)/SCOUT-O3 flights in the Sahel in August 2006 [*Cairo et al.*, 2009]. Although *Schiller et al.* [2009] find evidence of localized deep convective moistening to high levels (420 K), they conclude that on the whole their results confirm the Lagrangian studies.

[7] Dehydration of nascent stratospheric air has never been observed directly, and as in the study by *Vömel et al.* [2002], it must be inferred from limited observations. However, as *Peter et al.* [2006] have shown, significant supersaturation may occur in ice clouds near the tropical tropopause. Moreover, *Jensen et al.* [2005] and others have shown that significant supersaturation with respect to ice, even above the threshold for homogeneous nucleation, can be sustained in the absence of ice clouds. Thus, saturation, while necessary, is not a sufficient condition for dehydration. Nevertheless, the evidence from the water vapor tape recorder and the success of the Lagrangian approach would argue for the utility of the freeze-drying hypothesis, at least to first order.

[8] In this paper we report on two extended campaigns of balloon-borne measurements of water vapor and ozone launched from the radiosonde site of the National Meteorological Institute of Costa Rica (IMN) at Alajuela [10.0°N, 84.2°W]. These accompanied the NASA Tropical Convective System and Processes (TCSP) airborne mission in July 2005 [*Halverson et al.*, 2007] and the NASA Tropical Composition, Cloud, and Climate Coupling (TC4) experiment in July and August 2007 [*Toon et al.*, 2010]. During these two campaigns, a total of 38 launches were made with a payload that included the University of Colorado cryogenic frost point hygrometer or CFH [*Vömel et al.*, 2007a] and an electrochemical concentration cell (ECC) ozonesonde [*Komhyr et al.*, 1995]. The CFH is recognized as a reference instrument for water vapor measurements in the cold environment near the tropical tropopause and in the lower stratosphere and displays excellent agreement with the Aura Microwave Limb Sounder satellite water vapor measurement [*Vömel et al.*, 2007b].

[9] The TCSP and TC4 campaign CFH/ECC data sets provide an unprecedented opportunity to examine the short time scale variability of the structure of water vapor and ozone in the tropical upper troposphere and lower stratosphere (UT/LS) during periods of widespread regional convection. (For a meteorological overview of the TC4 campaign, see *Pfister et al.* [2010]). Furthermore, we place our analysis in the context of the evolution of the dynamical structure of the UT/LS using radiosondes launched 4 times daily from the IMN site in campaigns concurrent with the water vapor and ozone balloon sondes. With the radiosonde data we can explore the role of convectively driven equatorial waves in temperature variations of the TTL in general and the cold point tropopause (CPT) in particular. As we will show, the waves in the UT/LS are of sufficient amplitude such that on certain occasions the CPT will be in the lower stratosphere in air that is already extremely dry. This observation implies that the mixing ratio observed at the CPT is not always the best estimate of the stratospheric entry value for water vapor. We instead look for the layer near the tropopause in which saturation occurs and use the minimum mixing ratios in this layer to estimate the effective stratospheric entry value. We will refer to this layer as the

tropopause saturation layer or TSL and will show that it leads to a significantly lower, and physically more meaningful, estimate of the stratospheric entry value of water vapor than a cold point-based estimate.

[10] In section 2 we describe the balloon sonde and radiosonde data. Section 3 examines the mean structure and variability of temperature, ozone, and water vapor from the CFH/ECC sondes in the two campaigns, whereas section 4 focuses on the detailed structure of six representative balloon soundings in the TCSP campaign. In section 5 we examine wave-induced variability in the UT/LS and its relationship to temperature anomalies near the tropopause using the radiosonde temperature and wind data. Section 6 discusses the results and presents our conclusions.

2. Data

[11] The Ticosonde/Aura-TCSP (TCSP) project ran from June through August 2005 and the Ticosonde/TC4 project June through August 2007. Each was composed of a series of CFH/ECC balloon sondes to measure profiles of water vapor and ozone to the middle stratosphere and a regular program of radiosonde launches. The balloon sonde campaigns took place over periods of two and one-half weeks and a month, respectively, with 23 CFH/ECC ascents during TCSP and 15 during TC4. Radiosondes were launched 4 times daily at 0000, 0600, 1200, and 1800 UT from mid-June and to mid- or late August.

2.1. Water Vapor-Ozone Balloon Sondes

[12] The balloon sonde payload combined the CFH with the ECC ozonesonde; a Garmin GPS provided winds. The CFH is a lightweight (400 g) microprocessor-controlled instrument and operates on the chilled-mirror principle using a cryogenic liquid as cooling agent. It includes several improvements over the similar NOAA/CMD instrument [*Vömel et al.*, 2002] allowing it to measure water vapor continuously from the surface to about 28 km altitude. The accuracy in the troposphere is better than 5%, and the stratospheric accuracy is better than 10%. The CFH is capable of measuring water vapor inside clouds but may occasionally suffer from an artifact in which the optical detector collects water or ice. This condition leads to a malfunction of the instrument controller that is easily identified and thus can be screened out of the processed data.

[13] The ECC ozonesonde measures ozone by reaction with I_2 in a weak aqueous solution, the electrical current generated being directly proportional to the amount of ozone pumped through the cell. The accuracy of the ozone mixing ratio is typically ~5% and slightly lower at low ozone mixing ratios.

[14] During flight the CFH, ECC, and GPS data streams were transmitted to the ground-receiving equipment through an interface with a Vaisala RS80 radiosonde; the latter's pressure, temperature and relative humidity data stream was also captured. During TCSP, a Vaisala RS92-SGP was also added to the payload for the purposes of intercomparison of the RS92 twin-humicap relative humidity measurement with that from the CFH. As reported previously by *Vömel et al.* [2007c], this revealed a dry bias of the RS92-SGP relative humidity due to solar radiation approaching 50% at 15 km.

[15] The CFH/ECC payloads weighed approximately a kilogram and were flown from a 1200 g latex balloon filled with helium. Each balloon was equipped with a parachute so that data could be taken on descent as well as allow for the potential recovery of the instruments. (Only the ascent data are analyzed here, however.) Payload preparation and sonde launches were conducted by a team of students from the National University (UNA) of Costa Rica under the leadership of two of us (Vömel and Valverde). The UNA team was assisted by IMN technical staff.

[16] The CFH/ECC launches in the 2005 TCSP campaign were made on 18 consecutive days near local noon (1800 UT) beginning 8 July. On each of the last 5 days of the campaign, ascents were also made near local midnight. All but three ascents reached altitudes of 27 km or more, the highest altitude being 32.2 km. Of the 23 flights, 20 had good water vapor ascent data above 10 km, and on 14 of these, we obtained good data through the profile temperature minimum or higher.

[17] An initial launch for TC4 was made at local noon on 2 July 2007, but the intensive phase of the 2007 TC4 campaign began on 16 July with launches near local noon every 3 days through 31 July. There were an additional eight flights through 13 August, four of these taking place near local midnight (0600 UT). We have also included the noon launch on 30 August in our analysis. Table 1 lists the dates, times, and maximum altitudes of ascent data achieved in each of the flights.

2.2. Radiosondes

[18] The five Ticosonde radiosonde programs since 2004 are described in Appendix A, and the data and results from the Ticosonde/TC4 campaign in 2007 are discussed in the study by *Pfister et al.* [2010]. The Ticosonde/Aura-TCSP radiosonde campaign in 2005 began on 0000 UT 16 June and continued through 0000 UT 24 August. Of the flights, 269 reached the 150 hPa level or higher for an average burst altitude of 25.6 km. The great majority of the ascents were made with the Vaisala RS92-SGP radiosonde, although in the final days of the campaign, these were substituted with Vaisala RS90-AG sondes on 19 occasions and the Vaisala RS80-15G sonde on five occasions.

2.3. Payload Time Response

[19] We estimate the response time of the CFH in the stratosphere to be on the order of 10 to a few tens of seconds. For the ECC ozonesonde, *Komhyr et al.* [1995] estimated a response time between 20 s and a minute. Thus, at ascent rates of 5–7 m s^{-1}, the response times of the two instruments are reasonably well matched over a scale of a few hundred meters.

3. Average Profiles and Variability From the Water Vapor and Ozone Soundings

[20] We calculated the mean profiles and variance for temperature, ozone volume mixing ratio, observed and saturated water vapor volume mixing ratio, and relative humidity over ice (RHi) from the CFH/ECC sonde ascent data. To calculate mean statistics, we interpolated each ascent to a 50 m altitude grid and then derived means and

Table 1. Flight Statistics for CFH/ECC Launches During the July 2005 Ticosonde/Aura-TCSP Campaign and July–August 2007 Ticosonde/TC4 Campaign[a]

Flight	Day	Time (UT)	Maximum Altitude (km)	
			Ozone	WV
		Ticosonde/Aura-TCSP 2005		
SJ001	7/8	18:08	30.2	11.0
SJ002	7/9	17:54	30.3	12.6
SJ003	7/10	17:58	31.7	8.5
SJ004	7/11	18:14	31.1	21.0
SJ005	7/12	18:10	30.5	21.6
SJ006	7/13	18:06	31.6	24.4
SJ007	7/14	18:15	31.4	12.6
SJ008	7/15	17:54	32.2	17.8
SJ009	7/16	18:12	30.7	24.1
SJ010	7/17	17:40	30.3	20.7
SJ011	7/18	17:43	30.1	12.6
SJ012	7/19	17:34	30.1	25.0
SJ013	7/20	18:46	27.3	18.5
SJ014	**7/21**	**5:58**	**19.1**	**12.3**
SJ015	7/21	17:39	29.4	4.9
SJ016	**7/22**	**5:28**	**30.5**	**23.5**
SJ017	7/22	17:33	30.2	19.3
SJ018	**7/23**	**5:28**	**18.6**	**14.8**
SJ020	7/23	18:47	31.8	27.5
SJ021	**7/24**	**5:34**	**30.6**	**25.1**
SJ022	7/24	17:23	21.0	21.0
SJ023	**7/25**	**5:34**	**30.8**	–
SJ024	7/25	17:27	28.7	21.8
		Ticosonde/TC42007		
SJ132	7/2	17:48	27.3	26.4
SJ135	7/16	18:25	30.3	21.4
SJ136	7/19	17:57	32.1	21.0
SJ137	7/22	17:48	30.4	21.3
SJ138	7/25	17:05	32.0	20.1
SJ139	7/28	17:36	14.0	14.0
SJ140	7/31	17:20	31.7	31.7
SJ141	**8/2**	**05:39**	**30.1**	**17.0**
SJ142	8/3	15:42	31.2	27.7
SJ143	**8/4**	**05:20**	**28.8**	**18.1**
SJ144	**8/5**	**05:32**	**30.0**	**17.1**
SJ145	**8/7**	**05:31**	**28.9**	**17.3**
SJ146	8/8	17:36	30.7	23.9
SJ147	**8/09**	**05:29**	**29.3**	**23.0**
SJ148	8/13	14:50	27.4	24.7
SJ149	8/30	17:07	32.3	21.9

[a]Flights in bold are nighttime ascents.

standard deviations, as well as the maximum and minimum at each grid level in each campaign sample.

3.1. Temperature Structure

[21] The results for temperature and ozone mixing ratio are shown in Figures 1a (TCSP) and 1b (TC4). Table 2 tabulates statistics for variables at the CPT for both campaigns. In terms of the average values, maxima, and minima for the variables shown in Table 2, the CPTs in the two campaigns differed only slightly, although the variability was somewhat lower in TC4. Thus, to a very good approximation, the CPT in both years was located at 100 hPa, 375 K potential temperature and an altitude of 16.6 km. These values are well within a standard deviation of the global average values for July in the tropical tropopause climatology of *Seidel et al.* [2001].

[22] The mean TCSP temperature profile becomes more stable above 15.1 km, 130 hPa, and 357 K, a feature common in the tropical UT/LS as noted by *Atticks and Robinson* [1983] and in numerous studies since. Here, N^2 increases rapidly by over a factor of 2; similar behavior is observed in TC4. However, the most striking feature of the temperatures in both campaigns is the sharp increase of temperature variability above the 355 K level, shown in Figure 1 in terms of temperature range (light gray profiles at right) and as variance in Figure 2a. This is especially pronounced in TC4 due to the strong inversions observed in the first week of August [*Pfister et al.*, 2010, Figure 16]. Thus, while the full range of temperatures below 15 km in the TCSP sample is nowhere greater than 4.2°C, it increases to over 12°C by 16.5 km, close to the mean cold point. This rapid increase in variance is substantially larger than the growth rate $e^{Z/2H}$ due to decreasing density [*Andrews et al.*, 1987, p. 193] and is consistent with upward propagation of wave energy from the troposphere into the lower stratosphere.

3.2. Ozone

[23] The mean profiles of ozone differ in the troposphere where there is 25%–35% more ozone during TC4 than in TCSP. Likewise, the variance is greater, as is shown in Figure 2b. However, both mean profiles show inflections at 350 K, and while the TC4 variance does not display the abrupt increase at 350 K seen in TCSP, the 350 K level during TC4 lies within a steep variance gradient beginning at ~345 K. Thus, in both instances, increases in ozone variance accompany the inflections in the mean profile. *Folkins et al.* [2002] and others have linked the latter to a transition from detrainment of low ozone air by the deepest convective clouds to a regime where the ozone balance is between vertical advection and chemical production. The large temperature variance however is a strong indication that while this may be a layer of limited convective mixing, it is nonetheless extremely dynamic. In addition to variability due to adiabatic motion, it is possible that horizontal transport from middle latitudes may be contributing to the increased ozone variance as well affecting the steepness of the vertical gradient mean ozone profile [cf. *Avallone and Prather*, 1996; *Folkins et al.*, 1999]. We will examine this possibility in a forthcoming paper.

[24] In the discussion below, we use ozone mixing ratio to identify air in the TTL that is of lower and midtropospheric origin and that which is of stratospheric origin. The correspondence of the inflection in the mean profile mixing ratio with marked gradients in ozone variance at 350 K in each campaign suggests that the mean ozone mixing ratio at 350 K provides a useful discrimination between the lower and middle troposphere and the TTL above. During TCSP, the 350 K mean ozone was 0.0463 ± 0.0114 ppmv, and in TC4, it was 0.0590 ± 0.0157 ppmv. As the error bars overlap, the average of the two is appropriate, and rounded to the nearest 0.01 ppmv, this gives a TTL ozone threshold value for both campaigns of 0.05 ppmv. There is no corresponding inflection point or variance gradient to define stratospheric air, so here we use the campaign mean values of the ozone mixing ratios at the mean CPT. Again, the two campaign means are not significantly different statistically (0.158 ± 0.064 ppmv and 0.145 ± 0.037 ppmv, respectively), and so by similar averaging and rounding, we obtain a minimum stratospheric threshold value of 0.15 ppmv. "Transitional" air, i.e., air typical of the TTL, will be then

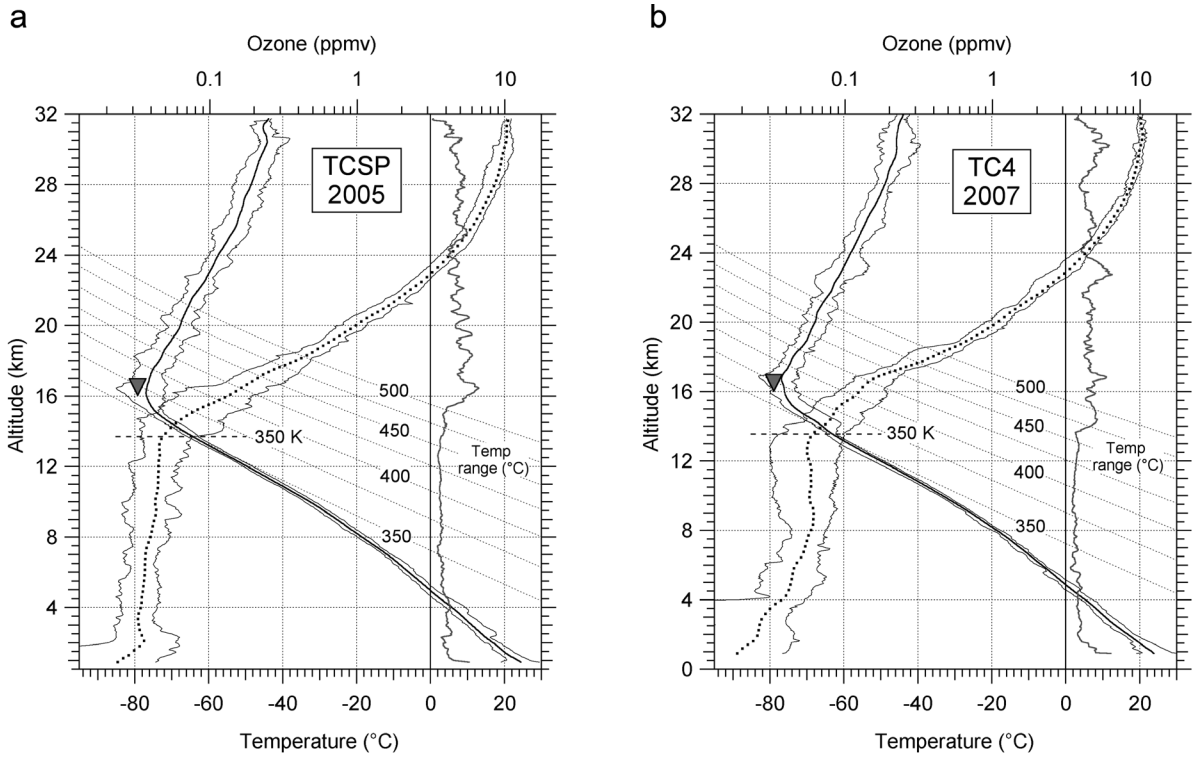

Figure 1. Campaign-mean profiles of temperature (heavy solid) and ozone mixing ratio (heavy dotted) for (a) TCSP and (b) TC4 calculated on a 50 m grid, each bracketed by the minima and maxima observed at each grid level in the campaign. Isentropes every 25 K between 350 and 500 K shown with dotted lines, and gray lines at right are profiles of the full range of temperatures in each campaign. Inverted triangles mark the mean altitude and temperature of the cold point tropopause.

defined as having ozone mixing ratio values between 0.05 and 0.15 ppmv.

3.3. Water Vapor

[25] Figure 3 displays the CFH water vapor volume mixing ratio data for each flight series and their mean profiles along with profiles of saturation water vapor mixing ratio and relative humidity over ice. The saturation mixing ratio is derived from the Vaisala RS80 pressure and temperature data using the Goff-Gratch formula for the saturation vapor pressure over ice [*Goff and Gratch*, 1946]. For display purposes we have smoothed the mean profiles to filter out fluctuations with scales less than a few hundred meters. We also plot the envelope of ±1 standard deviation of the water vapor, similarly smoothed. Finally, we plot the mean cold point in altitude and water vapor mixing ratio. In

Table 2. CPT Statistics for the TCSP and TC4 Water Vapor/Ozonesonde Flight Series

	Instrument	Units	Average	Standard Deviation	Minimum (or Lowest)	Maximum (or Highest)	*n*
			TCSP 8–25 Jul 2005				
Altitude	RS80	km	16.64	0.65	15.80	18.26	23
Pressure	RS80	hPa	99.9	10.6	114.6	75.2	23
Temperature	RS80	°C	−79.2	2.48	−85.0	−76.2	23
Potential temperature	RS80	K	375.3	13.6	360.1	403.9	23
Ozone mixing ratio	ECC	ppmv	0.158	0.064	0.056	0.288	22
Water vapor mixing ratio	CFH	ppmv	5.73	1.72	2.62	8.23	13
Saturation mixing ratio	RS80	ppmv	6.76	2.61	2.29	11.3	23
RHi	CFH/RS80	%	88.4	28.4	47.3	134.6	13
			TC4 2 Jul to 30 Aug 2007				
Altitude	RS80	km	16.64	0.56	15.78	17.55	15
Pressure	RS80	hPa	99.6	9.74	114.8	85.0	15
Temperature	RS80	°C	−78.9	1.69	−83.0	−77.0	15
Potential temperature	RS80	K	376.0	10.6	360.5	395.3	15
Ozone mixing ratio	CFH	ppmv	0.145	0.0366	0.097	0.23	15
Water vapor mixing ratio	ECC	ppmv	5.79	1.28	3.87	8.08	15
Saturation mixing ratio	RS80	ppmv	6.79	1.77	3.44	9.39	23
RHi	CFH/RS80	percent	89.0	21.9	53.9	119.3	15

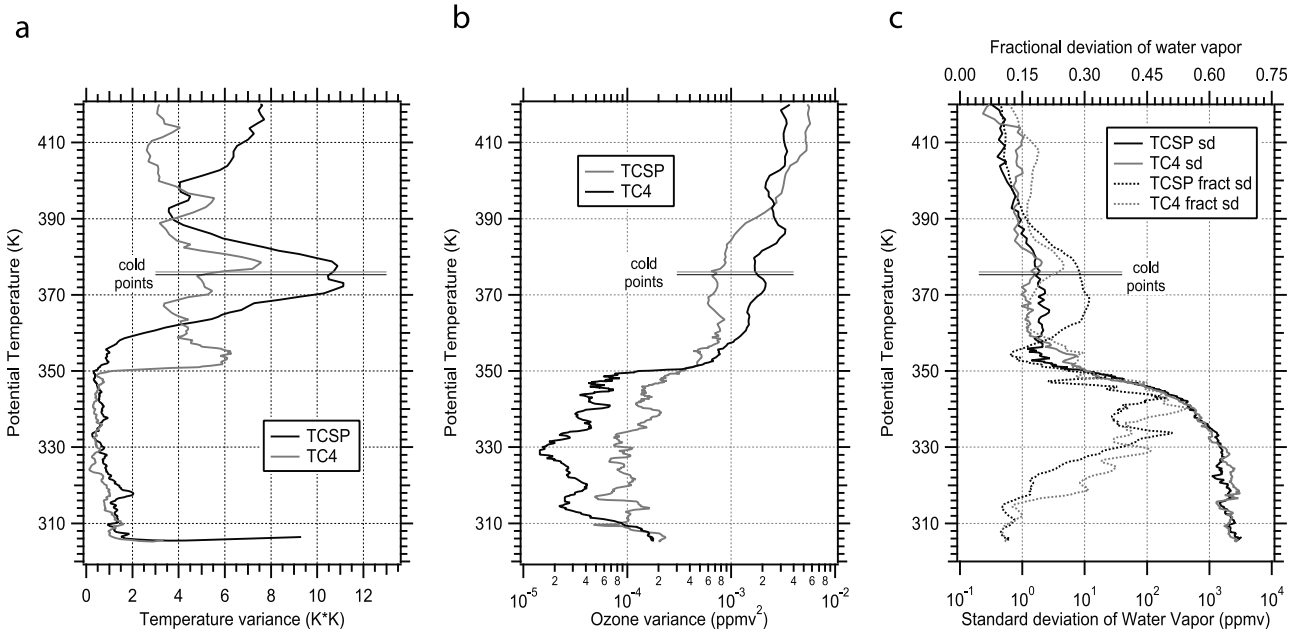

Figure 2. Variance of (a) temperature and (b) ozone mixing ratio and (c) standard and fractional deviations (see text) of CFH water vapor mixing ratio plotted against potential temperature. Horizontal lines are mean altitudes of the cold point tropopause from each campaign.

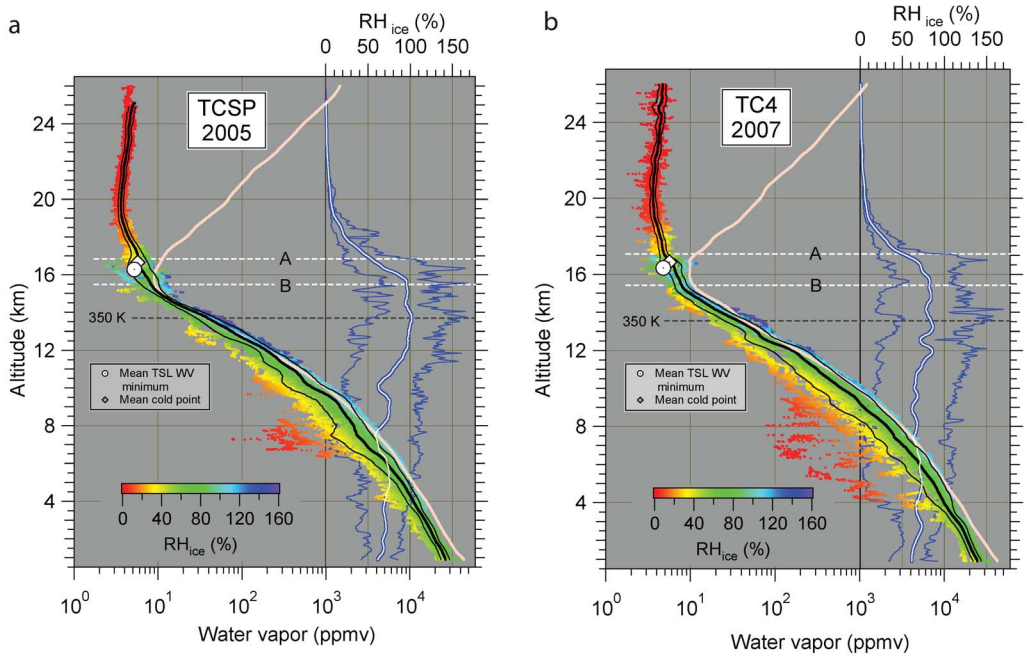

Figure 3. Water vapor and RHi profiles for (a) TCSP and (b) TC4. At left, water vapor volume mixing ratio data from each ascent color-coded by RHi; mean profile, heavy line; envelope of ± 1 standard deviation, thin lines; mean saturation mixing ratio, heavy pink line; mean water vapor minimum in the TSL, white circle; and mean cold point, white diamond; mean altitude of the 350 K surface, horizontal dashed gray line; and upper and lower bounds of tropopause saturation layer, dashed white lines A and B. At right, the mean profile of RHi, blue/white line; envelope of RHi maxima and minima, thin blue lines. All profiles except the RHi maxima and minima are smoothed in height (see text).

Table 3. Profile Minimum Water Vapor Statistics for the TCSP and TC4 Water Vapor and Ozonesonde Campaigns

	Instrument	Units	Average	Standard Deviation	Minimum (or Lowest)	Maximum (or Highest)	*n*
				TCSP—Jul 2005			
Altitude	RS80	km	19.5	0.72	18.3	20.7	12
Pressure	RS80	hPa	62.1	7.24	74.5	50.0	12
Temperature	RS80	°C	−69.5	2.63	−72.6	−64.5	12
Potential temperature	RS80	K	451.6	19.7	423.3	486.5	12
Water vapor	CFH	ppmv	3.21	0.47	2.7	4.4	12
Ozone	ECC	ppmv	0.79	0.27	0.464	1.36	12
				TC4—Jul/Aug 2007			
Altitude	RS80	km	20.3	1.12	19.0	23.0	11
Pressure	RS80	hPa	54.3	9.45	65.9	34.7	11
Temperature	RS80	°C	−67.2	3.22	−71.9	−61.4	11
Potential temperature	RS80	K	476.7	33.4	443.2	553.2	11
Water vapor	ECC	ppmv	3.02	0.56	1.84	3.57	11
Ozone	CFH	ppmv	1.27	0.772	0.66	3.25	11

Figures 3a and 3b, at right, we show the smoothed mean profile of relative humidity over ice within its envelope defined by the campaign maxima and minima at each grid level.

[26] Above 5 km (a level at or very close to the 0°C point in each campaign), the vertical structure of the water vapor was characterized by an unsaturated layer between 5 and 10 km with a mean RHi of 50%–75% and frequent instances of very dry air (RHi < 10%), a nearly saturated upper-tropospheric layer with saturation frequently exceeding 140% or more between 12 and 16 km and above 16 km a layer encompassing the CPT. In the latter, the mean RHi and the incidence of supersaturation decline rapidly.

[27] *Kley et al.* [1982] first showed that the minimum water vapor volume mixing ratio in this region and season is not located at the tropopause but well into the stratosphere; this is now understood to be a consequence of the water vapor tape recorder carrying up the lower water vapor mixing ratios emerging from the tropical tropopause in the northern winter season. Table 3 presents statistics of the stratospheric water vapor minima for the two campaigns. It lay somewhat lower than TC4 during TCSP at 19.5 km, 62.1 hPa, and 451.6 K potential temperature with value of 3.2 ppmv. The respective values for TC4 were 20.3 km, 54.3 hPa, 476.7 K, and 3.0 ppmv. Standard deviations at the profile minima (0.47 and 0.56 ppmv, respectively) were similar. The AMMA/SCOUT-O3 campaign over West Africa also took place during the northern summer but in 2006. While *Schiller et al.* [2009] (Figure 2c) show a shallow minimum in the stratospheric profile between 450 and 470 K that is comparable in altitude to the minimum here, their minimum mean water vapor mixing is approximately 1 ppmv higher.

[28] As can be seen in Figure 2c, in both campaigns, the vertical structure of the variability of water vapor is generally opposite to that observed in temperature and in ozone, with a rapid drop in the upper troposphere above ~335 K (~8 km) and a leveling off between 350 and 360 K. The large range of values of water vapor tends to obscure fine aspects of this vertical structure, so we have also plotted the standard deviations normalized by the mean profile. We call this the fractional deviation, and both the TCSP and TC4 profiles of this quantity maximize in the upper troposphere, roughly defining the layers of the maximum frequency of observed supersaturation. Above 355–360 K, the fractional deviation profiles have secondary peaks in each campaign, a broad one in TCSP peaking just below the mean cold point and a narrower one in TC4 at and just above the mean cold point; the latter is colocated with a local maximum in temperature variability. Thus, the strong increase of variability of temperature and ozone above 350 K is paralleled by concomitant structure in variability in the water vapor; the strongest of the upward motions that are modulating temperature and displacing ozone are very likely also leading to dehydration. The opposite is the case below 350 K; water vapor variability is decoupled from adiabatic lifting and sinking motion and, we assume, more related to convective cloud activity.

[29] The maximum saturation profiles in Figure 3 show that the highest altitudes where saturation is observed are close to the mean altitude of the CPT. In TCSP, this level lay at 380 K (16.8 km and 95.2 hPa). In TC4, it was only slightly higher at 381 K (17.1 km and 92.1 hPa). These we use as estimates of the upper boundary of the TSL in each campaign. To estimate the lower boundary of the TSL, we search downward through each individual profile for its minimum water vapor data point. The minimum may occur at the same observation as the CPT (i.e., so long as the CPT lies within the TSL), but it can occur elsewhere. During TCSP the lowest minimum lies at 360 K (15.5 km and 122 hPa), and in TC4, it was at 359 K (15.4 km and 123 hPa).

[30] The average values for the water vapor minima in the TSL were 5.2 ppmv in TCSP and 4.8 ppmv in TC4 versus means of 5.7 and 5.8 ppmv for the CPTs. The average altitudes of the minima were 16.34 km and 16.27 km and were on average 329 and 239 m below the profile CPT, respectively. The TCSP and TC4 relative humidities with respect to ice at the minima were 65% and 63% respectively, compared to CPT values of 88% and 89%.

[31] These average water vapor minima are plotted with solid circles in Figure 3 and can be compared to the average cold points that are plotted with diamonds. The TCSP average TSL minimum equals the average stratospheric value just above 17.5 km and 400 K potential temperature that is above the TSL. Here there is a rapid narrowing of the mixing ratio range to typical stratospheric values (see Figures 1 and 2b). The TC4 average TSL minimum also intersects the mean profile at a point where the variability

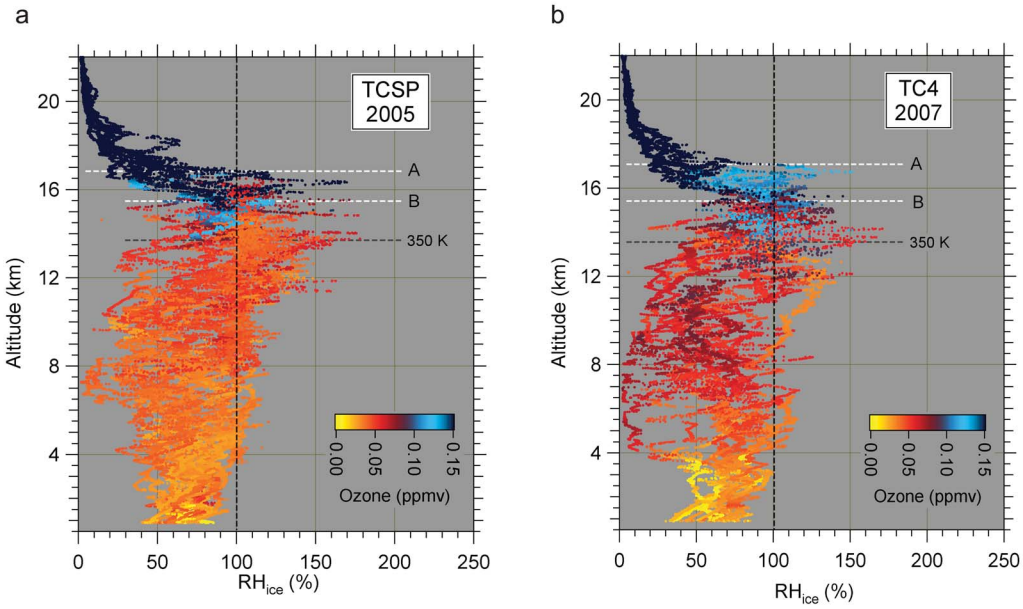

Figure 4. Observations of relative humidity with respect to ice (RHi) from (a) TCSP and (b) TC4, color-coded by ozone mixing ratio. Horizontal dashed lines as in Figure 3.

decreases substantially, although in this case, the intersection is at the top of the TSL. The significant point, however, is that these intersection points mark the transition from the high variability in water vapor associated with physical and dynamical processes in the TTL to the reduced and relatively constant variability of the stratosphere where further dehydration no longer occurs. With this as the threshold of the water vapor tape recorder, the TSL average minima are excellent estimates of the stratospheric entry value of water vapor mixing ratio, better than the averages defined at the CPT.

[32] The range of potential temperatures spanned by the TSL in each campaign, defined as they are in terms of the water vapor data alone, are remarkably similar. The TSLs are also similar in ozone content. Figure 4 displays the complete RHi data set for each of the two campaigns plotted against height. To distinguish air of stratospheric origin from tropospheric air, we color-coded each point according to its ozone mixing ratio. Data points with stratospheric ozone levels (>0.15 ppmv) are colored dark blue, and transitional air with ozone greater than 0.1 ppmv, a commonly used stratospheric threshold [*Thompson et al.*, 2003], is colored in lighter shades of blue. Lower tropospheric air (ozone levels < 0.05 ppmv) ranges from deep yellow to orange, and the lower range of transitional air (0.05–0.1 ppmv) spans orange to violet. We noted earlier that there were large differences in ozone between the campaigns in the troposphere (see Figure 1), and while the highest ozone mixing ratio in TCSP observed below 345 K was 0.065 ppmv, it was 0.91 ppmv in TC4. However, despite these interannual differences in ozone mixing ratio in the lower and middle troposphere, the TSLs in the two campaigns look very similar in three respects. First, we see no stratospheric air below 15 km in either campaign, and only on Flights 022 and 142 was stratospheric air observed below the TSL. Second, air with transitional ozone values occurred no higher than the upper edge of the TSL, and third, air with tropospheric ozone values, while occasionally found above the 350 K level, did not reach the TSL. This stands in contrast to the lower portion of TTL (the portion extending from the base of the TSL down to 350 K) where lower tropospheric ozone contents can be found but no stratospheric air.

[33] These observations suggest that while the TTL as a whole encompasses the entire transition in ozone mixing ratios from the tropical troposphere to the stratosphere, the saturation of nascent stratospheric air that must accompany final dehydration and thus "imprinting" on the water vapor tape recorder is restricted to the TSL. The TSL is unambiguously transitional in a thermodynamic sense in that it sits above the level of neutral buoyancy of the surface parcels with the greatest equivalent potential temperatures commonly found in the tropical marine boundary layer [*Selkirk*, 1993]. Only the rarest, most energetic convective systems are likely to penetrate into it and deposit boundary-layer levels of ozone and other trace constituents, and such was not observed in either of these campaigns.

[34] The TSL, defined here in terms of high-resolution sonde measurements at a single location and season in the tropics, may be just one form taken by the "tape head" of the satellite-derived water vapor tape recorder, a zonal mean entity. However, the TSL over Costa Rica lies in virtually the same potential temperature range as the tape head deduced by *Read et al.* [2004] and *Schoeberl et al.* [2006], so it may be that the TSL at Costa Rica is representative of convectively active regions in the tropics as a whole, at least in this season.

[35] As mentioned in section 1, the occurrence of saturation is only a necessary condition for dehydration, so there is no guarantee that the supersaturated layers in the TSL

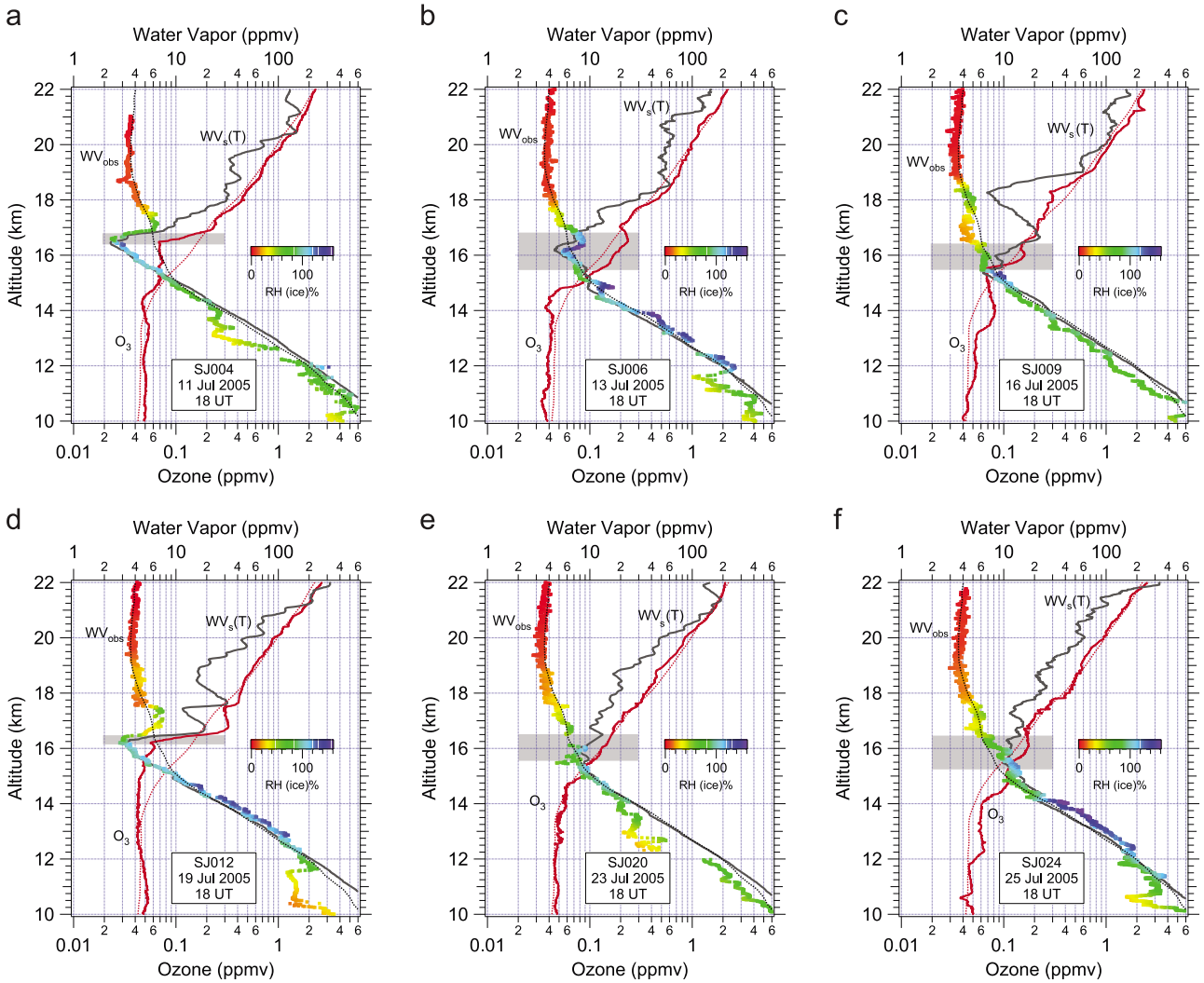

Figure 5. Selected ascents from the 2005 TCSP CFH/ECC campaign. Water vapor mixing ratio, heavy dots color-coded by relative humidity with respect to ice; mean water vapor mixing ratio, dotted black line; ozone mixing ratio, red line; mean ozone mixing ratio, dotted red line; and saturation mixing ratio of water, black line. Gray shading depicts depth of 360–380 K layer in each sounding. Soundings depicted were on (a) 11 July, (b) 13 July, (c) 16 July, (d) 19 July, (e) 23 July, and (f) 25 July.

over Costa Rica are associated with ongoing or even recent dehydration. On the other hand, the TSL is subject to radiative heating [*Gettelman and Forster*, 2002], and so TSL air sampled at Costa Rica will eventually exit the layer and be incorporated into the tape recorder, with the water vapor mixing ratio set within the TSL.

4. Characteristics of Individual Water Vapor and Ozone Profiles

[36] Figure 5 shows six profiles from the TCSP campaign that represent a range of behavior in water vapor mixing ratio, ozone mixing ratio, saturation mixing ratio, and RHi. As in Figure 3, we have color-coded the water vapor points according to RHi, and the campaign mean profiles of both water vapor mixing ratio and ozone mixing ratio are plotted to highlight regions of positive and negative anomalies. In addition, the 360–380 K layer that we have identified as the TSL is shown for each individual sounding.

[37] The profiles for 11 July (Figure 5a) and 19 July (Figure 5d) display the lowest minimum water vapor mixing ratios and the geometrically shallowest TSLs in the TCSP campaign. The minima occur at or very close to the CPT, reaching 2.34 ppmv at 16.6 km on 11 July and 2.68 ppmv at 16.2 km on 19 July. Both of these cold and dry tropopauses are at the upper edge of deep (>1 km) layers of anomalously low ozone (relative to the campaign mean) with mixing ratios in the lower end of the 0.05–0.15 ppmv transition range defined earlier. Of the two profiles, the 367.1 K potential temperature and 0.108 ppmv ozone mixing ratio at the 11 July minimum point are typical of the TSL, while the 19 July minimum, at 360.1 K and 0.056 ppmv sits at the lowest extreme among TSL air parcels. However, in both

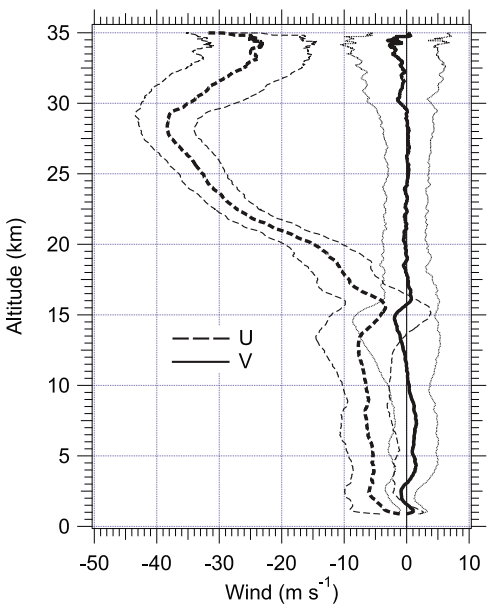

Figure 6. Mean profiles (heavy lines) of zonal (dashed) and meridional (solid) winds in envelopes of ±1 standard deviation (thin lines). Data from 4 times daily radiosondes at Alajuela over the 2 month period 16 June through 15 August 2005.

cases, the atmosphere immediately above the profile minimum shows both a strong temperature inversion and an extremely steep gradient in ozone mixing ratio, as much as 500 ppbv/km on 19 July. Trajectory analyses (not shown) for this case indicate that in an approximately 2 km layer centered at the tropopause, air had been following an anticyclonic path from the northeast for at least the previous 3 days. Likewise, air in the lower stratosphere had been following a similar trajectory, and the sharp tropopause gradient is unlikely to have been the result of a stacking of disparate layers. Thus, the tracer profiles in the TTL and the gradients above are consistent with uplift and adiabatic cooling below and descent of stratospheric air above.

[38] The sounding from 13 July (Figure 5b) shows supersaturation both in the upper troposphere between 12 and 15 km and in a layer within the TSL near the CPT. The upper layer contains stratospheric levels of ozone that are greater than the campaign mean, and the upper boundary of the layer lies above 380 K. It is unlikely that this combination of the supersaturation, stratospheric ozone, and high potential temperature could have been produced by penetrating convection. Soundings in Figures 5c and 5e (16 and 23 July, respectively) are subsaturated except for shallow layers near the tropopause. In the 16 July case, subsaturation in the upper troposphere from 13 to 15 km is accompanied by transitional levels of ozone and appears to be subsiding. The 23 July sounding is notable for an ozone profile that closely follows the mean profile, and the water vapor lies relatively close to the mean as well with only a small layer of supersaturation at 16 km. The sounding in Figure 5f (25 July) like in Figures 5b, 5c, and 5e is saturated in the TSL but at relatively high levels of water vapor and ozone. Below the TSL, transitional ozone levels extend down to 14.5 km where there is a sharp gradient with tropospheric levels in strongly supersaturated air down to nearly 12 km.

5. Temperature Variability and Coherent Fluctuations in the Upper Troposphere and the Lower Stratosphere

[39] We have shown in section 3 that in both campaigns the variability of temperature and ozone increases substantially above the 350 K potential temperature level, dramatically so in the case of TCSP. Here we show that the dominant modes of temperature variability above this level during both TCSP and TC4 lie in a spectrum of equatorial waves that are most likely excited by the deep convection in the region. *Pfister et al.* [2010] found that during the summer of 2007 when TC4 took place, these waves included modes on time scales of a week or more as well as higher frequency inertio-gravity waves. We focus on the wave variability observed during TCSP, during which the longer period modes were more dominant than in TC4.

[40] Upward propagation of equatorial waves is sensitive to wind shear. Figure 6 shows the profiles of the radiosonde mean zonal and meridional wind derived from the 4 times daily radiosonde launches at Alajuela for the 61 days between 0000 UT 16 June through 1800 UT 15 August 2005; the mean profiles are bracketed by envelopes of ±1 standard deviation. The profiles were obtained by interpolating the 2 s data from each sounding to a 10 m grid and then calculating mean profiles on this grid.

[41] The wind profiles in Figure 6 can be compared with the very similar features of the TC4 wind profiles in the study by *Pfister et al.* [2010], namely, east-southeasterly winds above the boundary layer that become easterly and then east-northeasterly, above 9 km in this case. The winds in 2005 also show increased variability in both components in the upper troposphere and mean northeasterly flow in the uppermost troposphere. The primary difference between 2005 and 2007 is that this upper tropospheric flow is stronger and extends through the mean cold point level. In the stratosphere, there is a similarly strong easterly shear that culminates in an easterly wind maximum of 42 ms^{-1} at 30 km.

[42] Figure 7 displays time-height cross sections of temporal anomalies of the radiosonde temperature (T'), zonal wind (u'), and meridional wind (v') for the same period as in Figure 6. Before plotting we took each grid-level time series and subtracted the 61 day mean and removed any linear trend. In addition, the data in the figures was smoothed in the vertical to substantially reduce variations at scales shorter than ~1 km. For reference purposes, we also plot the campaign mean heights of CPT and the 350 and 355 K potential temperature levels and, in addition, along the bottom edge of each plot arrows at the times of the 23 ascents of the CFH/ozonesonde payload between 8 and 25 July.

[43] Figure 7a is the time-height cross section of the T anomalies. While there is very little coherent variation below 350 K, above this level, and up to at least 21 km, there is an unmistakable pattern of downward propagating anomalies at periods of 4–16 days and vertical wavelengths of 4–5 km. In Figure 7a we have drawn dashed and dotted

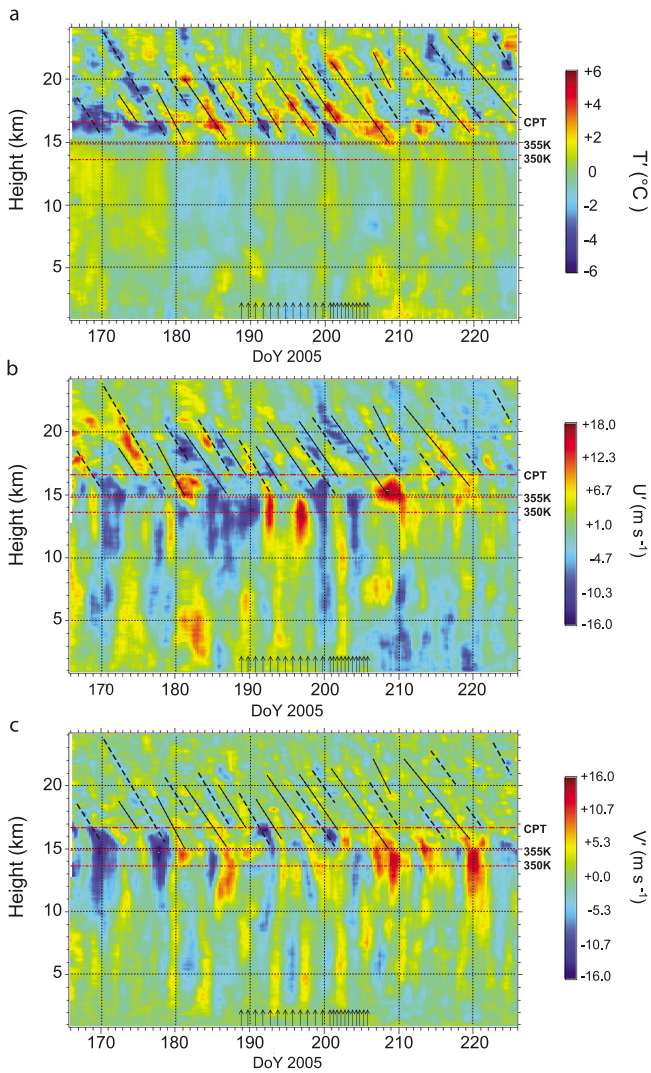

Figure 7. Time-height cross section of anomalies at Alajuela, 16 June to 15 August 2005 of (a) temperature, (b) zonal wind, and (c) meridional wind. Heavy dashed lines are phase lines of negative temperature anomalies; dotted lines indicate positive anomalies. Horizontal dotted lines at TCSP campaign (8–25 July) at the mean altitudes of the 350 and 355 K surface, and heavier dotted line at the mean altitude of the cold point tropopause. Arrows at bottom correspond to times of launches.

phase lines to highlight the descending cold and warm anomalies. The largest temperature anomalies occur between 355 K and the level of the mean CPT, although anomaly amplitudes of 4 K occur on several occasions near the 24 km level.

[44] Figures 7b and 7c show time-height cross sections of *u* and *v* anomalies, respectively. Both show very different behavior in the troposphere below 355 K where anomalies are vertically aligned; in the lower troposphere, easterly wave pulses of the meridional wind are particularly regular. In the UT/LS, the meridional wind appears to be in phase with the temperature anomalies, i.e., cold anomalies are accompanied by northerly wind anomalies, whereas the zonal wind anomalies appear to be in quadrature.

[45] As these waves impact the temperature at the tropopause, they have an effect on the saturation mixing ratio of water vapor. Figure 8 shows the time series of the saturation mixing ratio at the CPT during the 2005 campaign. (*Pfister et al.* [2010] present the corresponding time series for the summer of 2007.) The time series exhibits both high-frequency variability and peak-to-peak variations of up to 4 ppmv at time scales of ~5 days mixed with periods twice that; these become prominent after an extended low period in the first 10 days of the record (mid to late June). We have also plotted in Figure 8 the shorter record of water vapor mixing ratios from the gridded CFH sounding data (8–25 July). As we have already shown in the previous section, the cold point during TCSP was supersaturated more often than not. Thus, it is not surprising to note that the water vapor measurements in almost all cases exceed the saturation mixing ratio. Nevertheless, the sense of the synoptic scale variations in the saturation mixing ratio time series is preserved in the CFH data; in particular, there are saturation mixing ratio minima near days 192 and 201 that correspond to the strongly dehydrated profiles on 11 and 19 July.

[46] The results of spectral analyses of the temperature and winds are shown in Figure 9. They support the inferences from Figures 6 and 8. First, centered at 16 km, i.e., somewhat below the mean level of the CPT, the temperature shows a peak at periods centered at 4 days and a broader peak centered between 8 and 16 days. The 4 day feature extends upward through the CPT to just above 18 km as does power at periods longer than 16 days. Above 25 km, there is considerable power at a wide range of time scales longer than the inertial period (2.88 days at 10° latitude) but relatively little power between 20 and 25 km except for a weak feature in the 20–22 km region at ~5 days. Neither the zonal nor the meridional wind show as much spectral power at and above the tropopause relative to their variability in the troposphere, despite the clear features appearing in the time-height cross sections in Figure 7. However, the zonal wind power is dominated in the upper troposphere by roughly the same periods as the temperature shows at the tropopause and the lower stratosphere. Likewise the meridional wind shows a particularly strong feature at 4 days that is shifted only slightly downward in altitude relative to the temperature. Unlike the other two variables, the meridional wind shows some power in the inertial range in the upper troposphere, as well as strong variability in the low to midtroposphere due to easterly waves.

[47] Returning to the interrelationships between the components, the in-phase relationship between temperature and meridional wind in Figure 7 is supported by the results of cross-spectral analysis (not shown) that display peaks near 16 km in the *T*-*v* cospectrum at periods of 5 and ~10 days. Likewise, the quadrature relationship between temperature and zonal wind is reflected by peaks in the *T*-*u* quadrature spectrum at 5 days and 17 km and upward to ~20 km and also between 8 and 16 days above 15 km, again peaking at the 16 km level. This pattern of coherence between these components is characteristic of mixed Rossby-gravity waves [*Dunkerton and Baldwin*, 1995] that propagate westward and will rapidly decay with height in the presence of easterly shear. Such is the case with the spectral power in *T*, *u*, and *v* in both 2005 and 2007, each of these being in an easterly

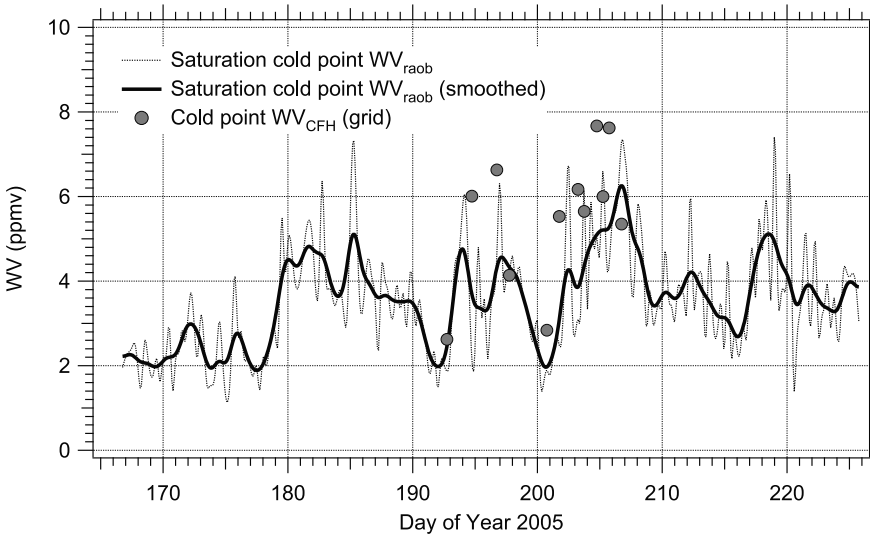

Figure 8. Time series of saturation mixing ratio at the cold point from radiosonde measurements at Alajuela, 16 June through 15 August 2005, light dotted line; spline-interpolated data binomially smoothed to highlight time scales longer than the diurnal, heavy line. Large dots are cold point water vapor volume mixing ratio from the CFH.

phase of the quasi-biennial oscillation [*Baldwin et al.*, 2001].

[48] The energy source for the waves is very likely regional deep convection. First, there is the sharp transition at 15 km from vertical coherence in the wind anomalies in the troposphere to downward phase propagation in all components above. This is consistent with energy propagating upward and away from the detrainment level for regional convective systems. Second, the coherent wave structure in the UT/LS, while a feature of the summer convective periods in Costa Rica in 2005 and 2007 reported here, was not repeated in the winter of 2006 when we conducted an extended radiosonde campaign at Alajuela in support of the NASA CR-AVE mission. During the winter dry season, deep convection is centered well south of the equator in tropical American longitudes, whereas during

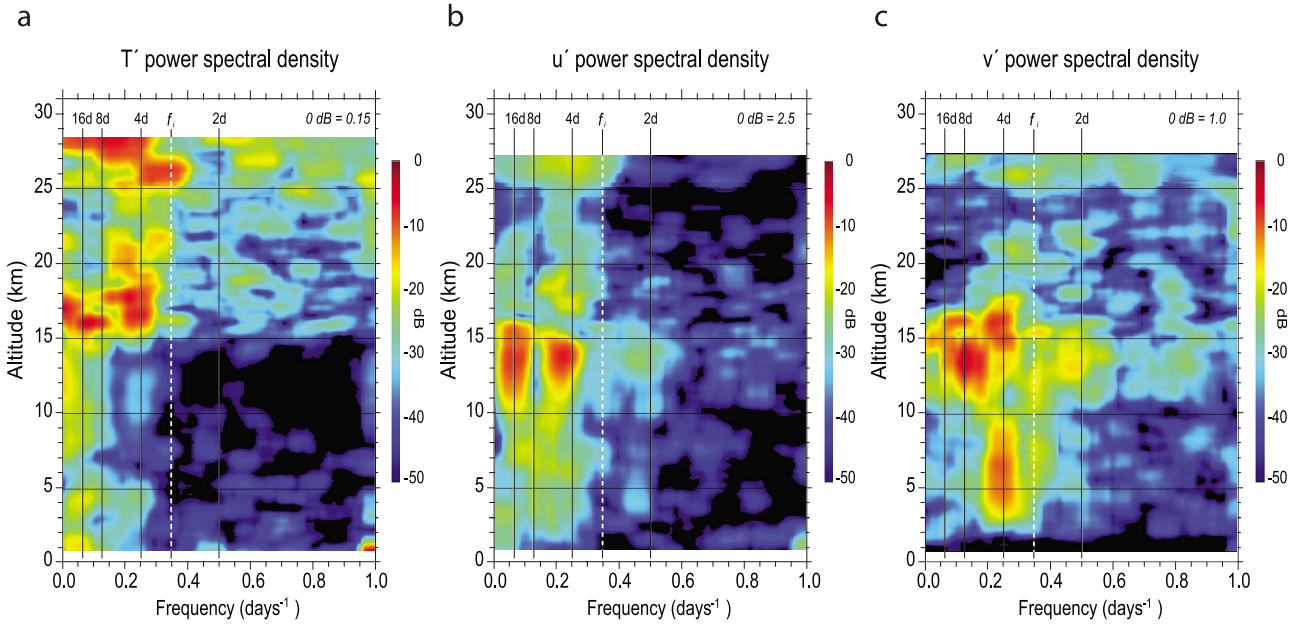

Figure 9. Frequency-height cross sections of power spectral density from periodogram analysis for anomalies of (a) temperature (T'), (b) zonal wind (u'), and (*c*) meridional wind (v') at Alajuela, 16 June to 15 August 2005. Equivalent periods in days are shown across the top; f_i marks the inertial period at 10°N.

summer, convection is maximized near the latitude of Costa Rica [*Pfister et al.*, 2010].

6. Discussion and Conclusions

[49] The profiles of both water vapor and ozone are consistent with the vertical structure of each of these trace species in the tropics obtained previously with in situ water vapor observations by *Vömel et al.* [2002] and ozonesonde observations from SHADOZ [*Thompson et al.*, 2003]. That is, the TCSP and TC4 mean profiles show an inflection in ozone at 350 K potential temperature and a mean CPT close to 16.6 km and 375 K potential temperature with water vapor volume mixing ratios slightly less than 6 ppmv. Stratospheric minima in the mean profiles of water vapor from TCSP and TC4 were within 0.1 of 3.1 ppmv. These lay above 19.5 km and 450 K potential temperature, with the latter campaign's minimum 0.8 km and 25 K higher.

[50] Similar to the observations reported in the study by *Vömel et al.* [2002], ice supersaturation was observed on nearly all of the TCSP ascents between 10 km and the CPT, typically in layers several kilometers deep, with embedded regions of supersaturation >40% observed on several ascents. Supersaturated layers were observed in the upper troposphere during TC4 as well, although not as frequently. In both campaigns the saturated layers included a subgroup with significant stratospheric fractions of ozone, though almost all of the latter were observed no lower than the 360 K level in either campaign.

[51] The close spacing of water vapor and ozone profiles we obtained in TCSP, and again in TC4, together with the 2 months plus records of high-frequency radiosondes enable us to unequivocally link the structure and variability in the trace constituents to equatorial waves. The profiles in the TCSP and TC4 campaigns each display similar vertical structures in temperature variability, with a marked increase in the variability of temperature at 355 K (14.9 and 14.5 km, respectively). This increased variability reflects adiabatic temperature changes associated with a spectrum of equatorial wave motions, including most significantly westward moving waves with time periods of 4 days and longer. Although not shown explicitly here, ozone anomalies above 15 km were likely also to have been induced by the vertical motion in the waves.

[52] Variability in temperature and ozone mixing ratio and the correlation of peaks in temperature and water vapor mixing ratio suggest that the layer between 360 and 380 K potential temperature is distinguished by significant in-mixing of stratospheric air and strong episodes of cooling resulting in dehydration. In contrast, the remainder of the TTL extending down to 350 K is only infrequently visited by air with stratospheric levels of ozone, defined here as a mixing ratio of 0.15 ppmv or greater. We have introduced the term tropopause saturation layer to refer to this upper portion of the TTL.

[53] Time-height cross sections of the radiosonde temperature and wind anomalies show that the cold episodes in the TSL occurred during cold phases of the equatorial waves as they propagated downward from the lower stratosphere to the ~15 km level. These temperature fluctuations were on the order of ±6 K in the stratosphere and likely led to dehydration events near the tropopause as well as variations of ozone due to vertical displacements across the steep mean gradient. In contrast, below the 15 km level, which is approximately the neutral buoyancy level for deep convection, the waves rapidly weakened with height, and water vapor variations become decoupled from the local temperature. In this region below the TSL, the observed supersaturations were most likely closely associated with detrainment of deep convective clouds and anvils. Similarly, the weakening of wave displacements in this convective regime below 15 km yields a marked decrease in the relative variability of ozone, and vertical mixing is the dominant process.

[54] Water vapor and ozone measurements were made in TCSP during two high-amplitude wave events that dehydrated the air to under 3 ppmv near the CPT. The second event, profiled in the sounding from 19 July (Figure 5d), is an example of tropopause-level dehydration appearing as the end stage of a process of slow ascent and cooling following deep convective detrainment several days upstream. In TC4, an unusual high-amplitude wave event in the first week of August not only pushed cold point water vapor down to 3 ppmv and below, but the accompanying adiabatic descent below the cold point produced a 3 km layer of ozone of constant 100 ppbv mixing ratio down to 14 km.

[55] As an organizing principle, the tropopause saturation layer is based on the Lagrangian assumption of *Jensen and Pfister* [2004], *Fueglistaler et al.* [2005], and others, i.e., the water vapor content of air parcels entering the stratosphere is determined primarily by their temperature history and not by the effects of penetrative convection. At any one point in a profile, that history will then reflect a local dehydration event upstream, i.e., wherever ascent forced by equatorial waves was sustained enough to cause saturation, ice cloud formation, and particle fallout. Second, we assume that we have enough soundings to derive a reasonable estimate of the maximum level at which saturation and dehydration have occurred, and from this, we can define an upper boundary in potential temperature of the layer of dehydration. Above this boundary, wave motions may affect the temperature profile but are insufficient to force further dehydration. Third, we have shown from the ozone data that rehydration by penetrative convection is minimal in the TSL, so that the water vapor mixing ratio of an individual air parcel dehydrated in the TSL is unlikely to rehydrate before it passes upward into the tape recorder.

[56] The consistency between the TSL minimum water vapor mixing ratios and the mixing ratios at the tape recorder threshold along with the high frequency of stratospheric air in the TSL are evidence that entry into the tape recorder is taking place during the summer season in Costa Rica. If this were not the case, then the mean TSL water vapor minima would have to have been substantially higher, outside the envelope of mixing ratios in the lower stratosphere.

[57] The TCSP and TC4 campaigns were very similar in regard to the gross characteristics of the vertical structure and variability of temperature, water vapor, and ozone. While there is an important difference between the campaigns in the lower mean RHi in TC4, it is consistent with the weaker convection overall in TC4 compared to TCSP (see Figures 5–7 in the study by *Pfister et al.* [2010]). The latter may also be related to the higher mean levels of ozone in the troposphere and its variability in TC4. In any event,

the similarities between the campaigns and to the results in the study by *Vömel et al.* [2002] suggest that our results in Costa Rica are relevant to wide regions of the tropics.

[58] The reproducibility between campaigns of detailed features of the TTL such as the cold point tropopause and the boundaries in potential temperature of the tropopause saturation layer is striking. This lends further support to our contention that deep convection is typically absent from the upper reaches of the TTL and that dehydration occurs in the TSL in wave-driven episodes of adiabatic uplift within an environment of slow, diabatic ascent. Further analysis of balloon sonde and other in situ data (perhaps combined with lidar and GPS radio occultation data) from other seasons and other regions will be required to show that the phenomenology of the TTL over Costa Rica during northern summer is seen elsewhere. The western Pacific and maritime continent region during northern winter comes immediately to mind. There the tropopause is substantially higher and colder than in Costa Rica during northern summer. Nevertheless, as convection only rarely reaches the tropopause in the tropics, wherever there are cooling events inducing adiabatic ascent, we expect that in situ water vapor measurements should reveal a distinct tropopause saturation layer within which can be diagnosed the stratospheric entry value of the water vapor mixing ratio.

Appendix A: Ticosonde Radiosonde Collaborations

[59] The Ticosonde/Aura-TCSP and Ticosonde/TC4 radiosonde launch campaigns were the second and fourth in a series of collaborations between investigators from NASA and Costa Rica to make intensive observations of atmospheric variability during the summer rainy season over Central America. The first campaign, Ticosonde/NAME, took place in the summer of 2004, and the third was a shorter (1 month) sonde campaign conducted in July 2006 called Ticosonde/Veranillo. All of the summer campaigns were focused on characterizing (1) the variability of temperature and winds in the UT/LS from inertial time scales up to the synoptic and (2) regional weather phenomena such as the veranillo or midsummer drought [*Magaña et al.*, 1999] and the Caribbean low-level jet [*Amador*, 1998; *Amador et al.*, 2006; *Amador*, 2008; *Muñoz et al.*, 2008], as well as temporal fluctuations in the TTL. Soundings from each campaign directly supported forecasting, flight planning, and analysis for the NASA TCSP and TC4 flight campaigns and with the CFH/ECC have also contributed to validation of measurements on board the NASA EOS Aura satellite and other platforms [e.g., *Vömel et al.*, 2007b; *Read et al.*, 2007]. In addition to these summer season campaigns, there was a winter campaign that took place in early 2006 in conjunction with NASA Costa Rica Aura Validation Experiment (CR-AVE).

[60] **Acknowledgments.** Funding for the Ticosonde project since 2004 at NASA has been provided through the Radiation Sciences Program, the Upper Atmosphere Research Project, the Atmospheric Chemistry Modeling and Analysis Program, and the Climate Dynamics Program. Donald Anderson (now at Johns Hopkins University), Michael Kurylo (now at the University of Maryland, Baltimore County), and Hal Maring of the Radiation Sciences Program were early advocates for and continuing supporters of this scientific collaboration between Costa Rica and the United States. The authors are grateful to Mark Schoeberl and Anne Douglass of the NASA Aura Science Team without whose support the CFH/SHADOZ Costa Rica launch program would never have become a reality. We would like to acknowledge the Costa Rica-USA Foundation (CRUSA) in Costa Rica, the National Science Foundation, and the NOAA Office for Global Programs for their support of the Ticosonde/NAME program and Ramesh Kakar of the NASA Atmospheric Dynamics program for his support of Ticosonde/TCSP. The Ticosonde data sets are a tribute to the enthusiasm and dedication of the launch teams from UNA, UCR, and IMN. In this regard, we are especially grateful to Victor Hernández at IMN; Victor Beita, Karla Cerna, Diana Gonzáles, and Jose Pablo Sibaja at UNA; and Kristel Heinrich, Marcial Garbanzo, and Gustavo Garbanzo at UCR. The Earth Science Project Office at NASA Ames Research Center has generously assisted the Ticosonde effort from the beginning and wish to thank Mike Gaunce, Mike Craig, and Marilyn Vasquez in particular. We also wish to acknowledge the important contributions in the field by Ticosonde Co-Investigators Jimena Lopez, formerly of the Bay Area Environmental Research (BAER) Institute, Sonoma, CA; Robert Bergstrom of the BAER Institute; Patrick Hamill of the San José State University, San José, CA; and Eladio Zárate, formerly of the National Meteorological Institute of Costa Rica and now at the Regional Committee on Hydrological Resources (CRRH). We are also thankful for the programming support at NASA Ames Research Center by Marion Legg and administrative support by Marion Williams and Mark Sittloh, all of the BAER Institute. We wish to thank Pedro León (now at Earth University) and Gustavo Otárola and their staff at the Costa Rican National Center for High Technology (CeNAT) who provided critical administrative and logistical support, as was also provided by the Regional Environmental Hub at the United States Embassy in San José and CRRH whose director is Max Campos. We thank Joan Alexander of Colorado Research Associates for useful suggestions and assistance in the cross-spectral analysis. Finally, we wish to thank the anonymous reviewers for very constructive critiques.

References

Amador, J. (1998), A climatic feature of the tropical Americas: The trade wind easterly jet, *Top. Meteorol. Oceanogr.*, *5*(2), 91–102.

Amador, J. A. (2008), The Intra-Americas Seas Low-Level Jet (IALLJ): Overview and future research, trends and directions in climate research, *Ann. N. Y. Acad. Sci.*, *1146*(1), 153–188.

Amador, J. A., E. J. Alfaro, O. G. Lizano, and V. O. Magaña (2006), Atmospheric forcing of the eastern tropical Pacific: A review, *Prog. Oceanogr.*, *69*, 101–142.

Andrews, D. G., J. R. Holton, and C. B. Leovy (1987), *Middle Atmosphere Dynamics*, 489 pp., Academic, San Diego, Calif.

Atticks, M. G., and G. D. Robinson (1983), Some features of the structure of the tropical tropopause, *Q. J. R. Meteorol. Soc.*, *109*, 295–308.

Avallone, L. M., and M. J. Prather (1996), Photochemical evolution of ozone in the lower tropical stratosphere, *J. Geophys. Res.*, *101*, 1457–1461.

Baldwin, M. P., et al. (2001), The quasi-biennial oscillation, *Rev. Geophys.*, *39*(2), 179–229.

Cairo, F., et al. (2009), An overview of the SCOUT-AMMA stratospheric aircraft, balloons and sondes campaign in West Africa, August 2006: Rationale, roadmap, and highlights, *Atmos. Chem. Phys. Discuss.*, *9*, 19,713–19,781.

Corti, T., B. P. Luo, Q. Fu, H. Vömel, and T. Peter (2006), The impact of cirrus clouds on tropical troposphere-to-stratosphere transport, *Atmos. Chem. Phys.*, *6*, 2539–2547.

Corti, T., et al. (2008), Unprecedented evidence for overshooting convection hydrating the tropical stratosphere, *Geophys. Res. Lett.*, *35*, L10810, doi:10.1029/2008GL033641.

Danielsen, E. F. (1982), A dehydration mechanism for the stratosphere, *Geophys. Res. Lett.*, *9*, 605–608.

Dunkerton, T. J., and M. P. Baldwin (1995), Observation of 3–6 day meridional wind oscillations over the tropical Pacific, 1973–1992: Horizontal structure and propagation, *J. Atmos. Sci.*, *52*, 1585–1601.

Folkins, I., M. Loewenstein, J. Podolske, S. J. Oltmans, and M. Proffitt (1999), A barrier to vertical mixing at 14 km in the tropics: Evidence from ozonesondes and aircraft measurements, *J. Geophys. Res.*, *104*, 22,095–22,102, doi:10.1029/1999JD900404.

Folkins, I., C. Braun, A. M. Thompson, and J. Witte (2002), Tropical ozone as an indicator of deep convection, *J. Geophys. Res.*, *107*(D13), 4184, doi:10.1029/2001JD001178.

Fueglistaler, S., and P. H. Haynes (2005), Control of interannual and longer-term variability of stratospheric water vapor, *J. Geophys. Res.*, *110*, D24108, doi:10.1029/2005JD006019.

Fueglistaler, S., M. Bonazzola, P. H. Haynes, and T. Peter (2005), Stratospheric water vapor predicted from the Lagrangian temperature history of air entering the stratosphere in the tropics, *J. Geophys. Res.*, *110*, D08107, doi:10.1029/2004JD005516.

Fueglistaler, S., A. E. Dessler, T. J. Dunkerton, I. Folkins, Q. Fu, and P. W. Mote (2009), Tropical tropopause layer, *Rev. Geophys.*, *47*, RG1004, doi:10.1029/2008RG000267.

Fujiwara, M., F. Hasebe, M. Shiotani, N. Nishi, H. Vömel, and S. Oltmans (2001), Water vapor control at the tropopause by the equatorial Kelvin wave observed over Galapagos, *Geophys. Res. Lett.*, *28*, 3143–3146.

Gettelman, A., and P. M. Forster (2002), A climatology of the tropical tropopause layer, *J. Meteorol. Soc. Jpn.*, *80*(4B), 911–924.

Gettelman, A., M. L. Salby, and F. Sassi (2002), Distribution and influence of convection in the tropical tropopause region, *J. Geophys. Res.*, *107*(D10), 4080, doi:10.1029/2001JD001048.

Goff, J. A., and S. Gratch (1946), Low-pressure properties of water from 160 to 212 F, *Trans. ASHVE*, *52*, 95–122.

Grosvenor, D. P., T. W. Choularton, H. Coe, and G. Held (2007), A study of the effect of overshooting deep convection on the water content of the TTL and lower stratosphere from Cloud Resolving Model simulations, *Atmos. Chem. Phys.*, *7*, 4977–5002.

Halverson, J., et al. (2007), NASA's Tropical Cloud Systems and Processes Experiment: Investigating tropical cyclogenesis and hurricane intensity change, *Bull. Am. Meteorol. Soc.*, *88*, 867–882.

Hartmann, D. L., J. R. Holton, and Q. Fu (2001), The heat balance of the tropical tropopause, cirrus, and stratospheric dehydration, *Geophys. Res. Lett.*, *28*, 1969–1972.

Highwood, E. J., and B. J. Hoskins (1998), The tropical tropopause, *Q. J. R. Meteorol. Soc.*, *124*, 1579–1604.

Holton, J., and A. Gettelman (2001), Horizontal transport and dehydration of the stratosphere, *Geophys. Res. Lett.*, *28*, 2799–2802, doi:10.1029/2001GL013148.

Jensen, E. J., O. B. Toon, H. B. Selkirk, J. D. Spinhirne, and M. R. Schoeberl (1996), On the formation and persistence of subvisible cirrus clouds near the tropical tropopause, *J. Geophys. Res.*, *101*, 21,361–21,375, doi:10.1029/95JD03575.

Jensen, E. J., and L. Pfister (2004), Transport and freeze-drying in the tropical tropopause layer, *J. Geophys. Res.*, *109*, D02207, doi:10.1029/2003JD004022.

Jensen, E. J., et al. (2005), Ice supersaturations exceeding 100% at the cold tropical tropopause: Implications for cirrus formation and dehydration, *Atmos. Chem. Phys.*, *5*, 851–862.

Jensen, E. J., A. S. Ackerman, and J. A. Smith (2007), Can overshooting dehydrate the tropical tropopause layer?, *J. Geophys. Res.*, *112*, D11209, doi:10.1029/2006JD007943.

Kley, D., A. L. Schmeltekopf, R. H. Winkler, T. L. Thompson, and M. McFarland (1982), Transport of water through the tropical tropopause, *Geophys. Res. Lett.*, *9*, 617–620.

Komhyr, W. D., R. A. Barnes, G. B. Brothers, J. A. Lathrop, and D. P. Opperman (1995), Electro-chemical concentration cell ozonesonde performance evaluation during STOIC 1989, *J. Geophys. Res.*, *100*, 9231–9244, doi:10.1029/94JD02175.

Konopka, P., et al. (2007), Contribution of mixing to the upward transport across the tropical tropopause layer (TTL), *Atmos. Chem. Phys.*, *7*, 3285–3308.

Liu, C., and E. J. Zipser (2005), Global distribution of convection penetrating the tropical tropopause, *J. Geophys. Res.*, *110*, D23104, doi:10.1029/2005JD006063.

MacKenzie, A. R., et al. (2006), Tropopause and hygropause variability over the equatorial Indian Ocean during February and March 1999, *J. Geophys. Res.*, *111*, D18112, doi:10.1029/2005JD006639.

Magaña, V., J. A. Amador, and S. Medina (1999), The midsummer drought over Mexico and Central America, *J. Clim.*, *12*, 1577–1588.

Mote, P. W., K. H. Rosenlof, M. E. McIntyre, E. S. Carr, J. C. Gille, J. R. Holton, J. S. Kinnersley, H. C. Pumphrey, J. M. Russell III, and J. W. Waters (1996), An atmospheric tape recorder: The imprint of tropical tropopause temperatures on stratospheric water vapor, *J. Geophys. Res.*, *101*, 3989–4006, doi:10.1029/95JD03422.

Mote, P. W., T. J. Dunkerton, M. E. McIntyre, E. A. Ray, P. H. Haynes, and J. M. Russell III (1998), Vertical velocity, vertical diffusion, and dilution by midlatitude air in the tropical lower stratosphere, *J. Geophys. Res.*, *103*, 8651–8666, doi:10.1029/98JD00203.

Muñoz, E., A. Busalacchi, S. Nigam and A. Ruiz-Barradas (2008), Winter and summer structure of the Caribbean low-level jet, *J. Clim.*, *21*, 1260–1276.

Newell, R. E., and S. Gould-Stewart (1981), A stratospheric fountain?, *J. Atmos. Sci.*, *38*, 2789–2796.

Peter, T., C. Marcolli, P. Spichtinger, T. Corti, M. B. Baker and T. Koop (2006), When dry air is too humid, *Science*, *314*, 1399–1402.

Pfister, L., et al. (2001), Aircraft observations of thin cirrus clouds near the tropical tropopause, *J. Geophys. Res.*, *106*, 9765–9786, doi:10.1029/2000JD900648.

Pfister, L., H. B. Selkirk, D. O'C. Starr, K. Rosenlof, and P. A. Newman (2010), A meteorological overview of the TC4 mission, *J. Geophys. Res.*, *115*, D00J12, doi:10.1029/2009JD013316.

Plumb, R. A., and M. Ko (1992), Interrelationships between mixing ratios of long-lived stratospheric constituents, *J. Geophys. Res.*, *97*, 10,145–10,156, doi:10.1029/92JD00450.

Read, W. G., D. L. Wu, J. W. Waters, and H. C. Pumphrey (2004), Dehydration in the tropical tropopause layer: Implications from the UARS Microwave Limb Sounder, *J. Geophys. Res.*, *109*, D06110, doi:10.1029/2003JD004056.

Read, W. G., et al. (2007), Aura Microwave Limb Sounder upper tropospheric and lower stratospheric H_2O and relative humidity with respect to ice validation, *J. Geophys. Res.*, *112*, D24S35, doi:10.1029/2007JD008752.

Reed, R. J., and C. L. Vleck (1969), The annual variation in the tropical lower stratosphere, *J. Atmos. Sci.*, *26*, 163–179.

Reid, G. C., and K. S. Gage (1981), On the annual variation in the height of the tropical tropopause, *J. Atmos. Sci.*, *38*, 1928–1938.

Reid, G. C., and K. S. Gage (1996), The tropical tropopause over the western Pacific: Wave driving, convection, and the annual cycle, *J. Geophys. Res.*, *101*, 21,233–21,241, doi:10.1029/96JD01622.

Schiller, C., J.-U. Grooß, P. Konopka, F. Plöger, F. H. Silva dos Santos, and N. Spelten (2009), Hydration an dehydration at the tropical tropopause, *Atmos. Chem. Phys.*, *9*, 9647–9660.

Schoeberl, M. R., B. N. Duncan, A. R. Douglass, J. Waters, W. Read and M. Filipiak (2006), The carbon monoxide tape recorder, *Geophys. Res. Lett.*, *33*, L12811, doi:10.1029/2006GL026178.

Schoeberl, M. R., A. R. Douglass, R. S. Stolarski, S. Pawson, S. E. Strahan, and W. Read (2008), Comparison of lower stratospheric tropical mean vertical velocities, *J. Geophys. Res.*, *113*, D24109, doi:10.1029/2008JD010221.

Seidel, D. J., R. J. Ross, J. K. Angell, and G. C. Reid (2001), Climatological characteristics of the tropical tropopause as revealed by radiosondes, *J. Geophys. Res.*, *106*, 7587–7878, doi:10.1029/2000JD900837.

Selkirk, H. B. (1993), The tropopause cold trap in the Australian monsoon during STEP/AMEX 1987, *J. Geophys. Res.*, *98*, 8591–8610, doi:10.1029/92JD02932.

Sherwood, S. C., and A. E. Dessler (2001), A model for transport across the tropical tropopause, *J. Atmos. Sci.*, *58*, 765–779.

Thompson, A. M., et al. (2003), Southern Hemisphere Additional Ozonesondes (SHADOZ) 1998–2000 tropical ozone climatology: 1. Comparison with Total Ozone Mapping Spectrometer (TOMS) and ground-based measurements, *J. Geophys. Res.*, *108*(D2), 8238, doi:10.1029/2001JD000967.

Thuburn, J., and G. C. Craig (2002), On the temperature structure of the tropical substratosphere, *J. Geophys. Res.*, *107*(D2), 4017, doi:10.1029/2001JD000448.

Toon, B., et al. (2010), Planning and implementation of the Tropical Composition, Cloud, and Climate Coupling Experiment (TC4), *J. Geophys. Res.*, *115*, D00J04, doi:10.1029/2009JD013073.

Vaughan, G., C. Schiller, A. R. MacKenzie, K. Bower, T. Peter, H. Schlager, N. R. P. Harris, and B. T. May (2008), SCOUT-O3/ACTIVE: High-altitude aircraft measurements around deep tropical convection, *Bull. Am. Meteorol. Soc.*, *89*, 647–662, doi:10.1175/BAMS-89-5-647.

Vömel, H., et al. (2002), Balloon-borne observations of water vapor and ozone in the tropical upper troposphere and lower stratosphere, *J. Geophys. Res.*, *107*(D14), 4210, doi:10.1029/2001JD000707.

Vömel, H., D. E. David, and K. Smith (2007a), Accuracy of tropospheric and stratospheric water vapor measurements by the cryogenic frost point hygrometer: Instrumental details and observations, *J. Geophys. Res.*, *112*, D08305, doi:10.1029/2006JD007224.

Vömel, H., et al. (2007b), Validation of Aura Microwave Limb Sounder water vapor by balloon-borne Cryogenic Frost Point Hygrometer measurements, *J. Geophys. Res.*, *112*, D24S37, doi:10.1029/2007JD008698.

Vömel, H., H. Selkirk, L. Miloshevich, J. Valverde, J. Valdés, E. Kyrö, R. Kivi, W. Stolz, G. Peng, and J. A. Diaz (2007c), Radiation dry bias of the Vaisala RS92 humidity sensor, *J. Atmos. Ocean. Technol.*, *24*, 953–963.

Wang, P.-H., P. Minnis, M. P. McCormick, G. S. Kent, and K. M. Skeens (1996), A 6-year climatology of cloud occurrence frequency from Stratospheric Aerosol and Gas Experiment II observations (1985–1990), *J. Geophys. Res.*, *101*, 29,407–29,429.

Yulaeva, E., J. R. Holton, and J. M. Wallace (1994), On the cause of the annual cycle in tropical lower-stratospheric temperature, *J. Atmos. Sci.*, *51*, 169–174.

J. Amador, Center for Geophysical Research, University of Costa Rica, San Jose 2060, Costa Rica.

J. A. Diaz and W. Fernández, School of Physics, University of Costa Rica, San Jose 2060, Costa Rica.

G. S. Peng, The Aerospace Corporation, PO Box 92957, M1/102, Los Angeles, CA 90009-2957, USA.

L. Pfister, Earth Sciences Division, NASA Ames Research Center, M/S 245-5, Moffett Field, CA 94035-1000, USA.

H. Selkirk, NASA Goddard Space Flight Center, Code 613.3, Greenbelt, MD 20771, USA. (henry.b.selkirk@nasa.gov)

W. Stolz, National Meteorological Institute, PO Box 5583, San Jose 1000, Costa Rica.

J. M. Valverde Canossa, School of Environmental Sciences, National University, PO Box 86, Heredia 3000, Costa Rica.

H. Vömel, Deutscher Wetterdienst, Meteorologisches Observatorium, Am Observatorium 12, D-15848 Lindenburg, Germany.